Lawrence Berkeley National Laboratory
Recent Work

Title
Magnetization reversal and local switching fields of ferromagnetic Co/Pd microtubes with radial magnetization

Permalink
https://escholarship.org/uc/item/0g15d6mc

Journal
Physical Review B, 99(9)

ISSN
2469-9950

Authors
Puwenberg, N
Reiche, CF
Streubel, R
et al.

Publication Date
2019-03-29

DOI
10.1103/PhysRevB.99.094438

Peer reviewed

eScholarship.org Powered by the California Digital Library
University of California

Magnetization reversal and local switching fields of ferromagnetic Co/Pd microtubes with radial magnetization

Norbert Puwenberg [1,5], Christopher F. Reiche [2], Robert Streubel [3], Mishal Khan [5], Dipankar Mukherjee [1,5], Michael Melzer [1], Oliver G. Schmidt [1,4], Bernd Büchner [1,5] and Thomas Mühl [1]

[1] IFW Dresden, Dresden, Germany
[2] University of Utah, Salt Lake City, USA
[3] Lawrence Berkeley National Laboratory, Berkeley, USA
[4] TU Chemnitz, Chemnitz, Germany
[5] Technische Universität Dresden, Dresden, Germany

Abstract

We spatially resolve the field-induced magnetization reversal of ferromagnetic microtubes utilizing multi-frequency magnetic force microscopy (MFM). The microtubes are composed of rolled-up Co/Pd multilayer films with perpendicular magnetic anisotropy. Simultaneously mapping the topography and perpendicular magnetostatic force derivative, the relation between surface angle and local magnetization configuration is evaluated for a large number of locations with slopes exceeding 45 degrees. The angle-dependence of the switching field is concurrent with the Kondorsky model, i.e. the rolled-up nanomembrane behaves like a planar magnetic film with perpendicular anisotropy and a pinning dominated magnetization reversal. Additionally, we discuss methodological challenges when detecting magnetostatic force derivatives near steep surfaces.

1 Introduction

Recent advances in synthesis science, theory, and instrumentation combined with novel electronics concepts have boosted the research interest into three-dimensional nanomagnetism [1] covering both non-collinear spin textures and curved magnetic geometries [2]. The expansion into the third dimension does not only allow for vertically stacking microelectronics (2.5 D architectures), but also launches new functionalities associated with curvature and shape. The effect of curvature and shape can be classified into three categories: i) curvature-induced vector spin exchange [3] and magnetochiral effects [4]; ii) topology-driven modifications; and iii) spin frustration and pinning in three-dimensional networks. These mechanisms are the foundation for revolutionary concepts, including tubular magnonic waveguides with an unidirectional, reconfigurable dispersion relation [5], azimuthally magnetized tubes with small magnetic anisotropy for giant magnetoimpedance-based magnetoencephalography [6], tubular channels for fuel-free transport of superparamagnetic beads [7], and domain wall propagation in three-dimensional racetrack memories [8].

The common theme of three-dimensional nanomagnetism is the governance of magnetic properties under the three-dimensional distribution of the magnetization configuration. Hence, a profound understanding of underlying mechanisms, and the optimization of device performance demand the visualization of magnetization configuration. Addressing the transformative challenge of imaging the magnetic vector field, numerous techniques have been developed and advanced, including high-resolution Lorentz microscopy [9], vector field electron tomography [10, 11], and magnetic x-ray microscopy and tomography [12, 13]. In addition to these expensive tools operated at large-scale user facilities, cost-efficient table-top setups have been explored based on magneto-optical Kerr effect magnetometry [14] and, as outlined in this work, multi-frequency magnetic force microscopy.

Here, we study Co/Pd microtubes composed of rolled-up multilayers. Co/Pd multilayers are sandwich-structured magnetic thin films, whose magnetic anisotropy, i.e. strength, type, and direction of a potential perpendicular magnetic easy axis, can be tailored via tuning the thickness of individual cobalt and palladium layers [15–17]. Our Co/Pd microtube samples are manufactured by means of strain-engineering of magnetic multilayer films with tube diameters in the micrometer range. The appeal of these three-dimensional ferromagnetic nanostructures ranges from prototypical systems for magnetic x-ray tomography [12] to experimental demonstration of theoretically predicted phenomena as already described above.

We investigate field-dependent magnetization processes of a radially magnetized Co/Pd microtube at the nanoscale facilitating multi-frequency MFM, and determine the model describing the reversal processes. The detection of magnetostatic force derivatives near steep surfaces with slopes beyond 45 degrees faces experimental limitations that can in future be overcome harnessing the recently introduced bidirectional mode of MFM operation [18, 19].

1.1 Magnetization reversal

The magnetic field-driven magnetization reversal in real systems can generally be approximated by either of three analytical models, revealing the underlying mechanism: (i) Stoner-Wohlfarth model

based on the coherent rotation of magnetic moments in very small particles [20, 21]; incoherent modes, such as curling- or buckling-type reversal in ferromagnetic nanowires [22–25]; and Kondorsky model referring to a pinning dominated reversal [26, 27]. Fig. 1 shows a comparison between a coherent rotation (Stoner-Wohlfarth model) and a pinning dominated reversal (Kondorsky model) in ferromagnetic samples.

The Stoner-Wohlfarth model considers only one (uniaxial) anisotropy axis, which is defined as the easy axis of magnetization. In the absence of an external magnetic field, the magnetization of the particle is aligned parallel to the easy axis. When an external magnetic field is applied, the new magnetic ground state is defined by the interplay between magnetic anisotropy and Zeeman energy, with the latter describing the interaction between the external magnetic field and the magnetic moment of the particle. The magnetic anisotropy of the particle gives rise to two local energy minima, separated by an energy barrier, which is symmetric at zero magnetic field and prevails for small external fields. For sufficiently large magnetic fields H, the barrier vanishes. When the external magnetic field is antiparallel to the initial magnetization, the system relaxes into the state with the nearest energy minimum, and thus, switching the magnetization. The field, at which magnetic switching occurs depends on the angle ϕ between external field and easy axis, and is called the angle-dependent switching field $H_S(\phi) = H_S(0°) \cdot (\cos^{2/3}\phi + \sin^{2/3}\phi)^{-3/2}$.
As mentioned earlier, this model is generally limited to a coherent, uniform magnetization rotation predominantly occurring in single domain particles with sizes of the order of 10 nm [28, 29]. However, the model may also describe the magnetization reversal process in larger structures like out-of-plane magnetized Co/Pt nanodots with lateral expansions up to 100 nm [30]. They revealed a Stoner-Wohlfarth like behavior of the angle-dependent switching field. In this case, $H_S(\phi)$ has the lowest value at an angle of 45° between applied field direction and easy axis of magnetization. For larger angles, however, Delalande et al. [30] could show that after reversing the magnetic field, the nanodots may form a pinned multi-domain state. Roy and Kumar also found a Stoner-Wohlfarth like angular dependence of the switching field $H_S(\phi)$ in Sr/Fe thin films with low density of magnetic inhomogeneities, that would act as pinning sites. They observed a minimal switching field at an angle close to 45° but, in contrast to the theoretical model, an asymmetric angular dependence with distinct $H_S(0°)$ and $H_S(90°)$ values. In general, larger-scaled ferromagnetic solids like thin films possess a multi-domain (MD) structure, in which the magnetic domains are separated by domain walls whose size is defined by the interplay of exchange interaction and magnetic anisotropy energy. A transition from a single-domain state to a state split up into multiple domains reduces magnetostatic stray field contributions and thus lowers the magnetostatic energy of the ferromagnet. The domain walls play an important role in the magnetization reversal in MD materials since magnetic switching processes involve nucleation of domains with reversed magnetization and a displacement of domain walls in the material, which can be hindered by magnetic inhomogeneities [31, 32]. Even when the external magnetic field is insufficient to reverse the magnetization through a coherent rotation of the magnetic moments in the material, the component of the applied magnetic field parallel to the easy axis of magnetization can push the domain wall through the ferromagnetic solid [32]. This results in a Kondorsky type behavior of the switching field $H_S(\phi) = H_S(0°) \cdot 1/\cos\phi$, which was observed, for example, by Roy and Kumar for Sr/Fe films with a large density of pinning sites and by Delalande et al. that investigated extended Co/Pt thin films [30, 32].

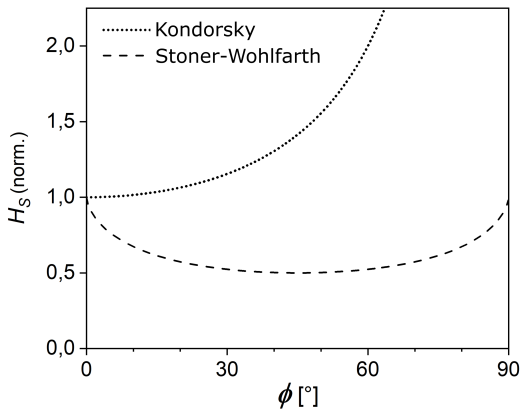

Figure 1: Simulated switching curves for Kondorsky ($H_S(\phi) = H_S(0°) \cdot 1/\cos\phi$) and Stoner-Wohlfarth ($H_S(\phi) = H_S(0°) \cdot (\cos^{2/3}\phi + \sin^{2/3}\phi)^{-3/2}$) type magnetization reversal. H_S is the switching field normalized to the switching field at 0°, at which $H_S(0°) = 1$ applies, and ϕ denotes the angle between the applied field and the easy axis of magnetization.

1.2 Multi-frequency MFM of curved surfaces

We use a dedicated MFM technique employing two superimposed flexural oscillation modes of the cantilever to simultaneously map the topography of the tubular surface and its magnetic stray-field landscape with high sensitivity and high spatial resolution. This multi-frequency ansatz was inspired by the work of J. Schwenk et al. [33] and offers the advantage of simultaneous recording during one single scan in a true non-contact measurement.

MFM in frequency-modulation mode takes advantage of the frequency shift Δf of a cantilever resonance as a direct measurement signal, which reflects the interaction between tip and sample [34]. A tip oscillating in z-direction is sensitive to the derivative of the tip-sample force z-component with respect to the normal spatial z-coordinate ($\partial F_z/\partial z$). Modeling the MFM tip as a perfect point dipole with a magnetic moment m_z along the z-axis, the relation between frequency shift and the z-component of the magnetostatic stray-field H_z emerging from a magnetically active sample can be expressed by [35]:

$$\Delta f = -\mu_0 \, m_z \, \frac{f_0}{2k} \, \frac{\partial^2 H_z}{\partial z^2} \, . \tag{1}$$

Here, f_0 denotes the resonance frequency of the cantilever and k its flexural stiffness. In MFM, the separation of magnetostatic contrast and sample topography is challenging and often realized by using dual-passage methods in air, in which each scan line is scanned twice. The first pass in intermittent tip-sample contact maps the topography, the second pass at an increased tip-sample distance provides sensitivity to magnetostatic tip-sample interactions [36–38].

The approach we use for microtube imaging employs multiple cantilever excitation frequencies and is capable to decouple magnetostatic interactions from the sample topography even for large height variations up to several micrometers and slopes well above 45°. In contrast to the aforementioned two-pass technique, the fundamental and second mode flexural cantilever oscillation serve as independent measurement channels that record magnetostatic and topographic information simultaneously in a single pass [33]. In our case, the amplitude of the second oscillation mode is used to control

the tip-sample distance [33]. The second mode oscillation is excited by applying an AC voltage $\hat{U}_{AC}$ between MFM tip and sample at half the eigenfrequency of the second cantilever eigenmode $f_{AC} = 1/2 \cdot f_2$. The tip-sample arrangement forms a capacitor with capacitance C_{ts}. The emergent electrostatic force component $F_{2f_{AC}}$ becomes [33]:

$$F_{2f_{AC}}(z) = -\frac{1}{4}\frac{\partial C_{ts}(z)}{\partial z}\hat{U}_{AC}^2 \, cos(2 \cdot 2\pi f_{AC} t) \; . \tag{2}$$

Both periodic force $F_{2f_{AC}}$ and second mode oscillation amplitude A_2 strongly depend on the tip-sample distance z_{ts} due to the $\partial C_{ts}/\partial z$ distance dependence. Thus, A_2 allows for controlling the tip-sample distance keeping the amplitude constant via a feedback loop. Another feedback loop locking the phase ensures that the second mode is excited at its resonance. This measure prevents crosstalk between force gradients, produced by magnetostatic interactions or contact potential differences, and the second mode amplitude and therefore on the distance control. Note that the amplitude-distance relation depends on the Q-factor of the driven oscillation, which in turn is affected by local changes of dissipative magnetization processes, potentially corrupting the distance control [33]. However, in our case, we did not observe a location dependence of the dissipation in the fundamental oscillation mode. Hence, guaranteeing a constant tip-sample distance by the second mode cantilever oscillation, the frequency shift of the mechanically excited fundamental mode Δf_1 can be used to map force gradients originating from the sample magnetostatic stray field distribution. In addition, the fundamental mode oscillation amplitude A_1 is kept constant by a PI controlled feedback loop. The result is a superposition of two oscillations at the corresponding resonance frequencies of fundamental and second cantilever mode with amplitudes maintained at a constant level.

2 Experimental techniques and MFM measurements

A ferromagnetic $[\mathrm{Co}(0.4\,\mathrm{nm})/\mathrm{Pd}(0.7\,\mathrm{nm})]_5$ multilayer stack with perpendicular anisotropy, fully saturated remanent state, and capped with 2 nm Pd forms the magnetic foundation of the investigated microtubes [12]. This magnetic multilayer film was subsequently sputter-deposited with a strained polycrystalline titanium layer with a thickness of 20 nm onto a lithographically patterned sacrificial photoresist layer [39]. The patterns consist of 20 x 20 μm squares with a period of 50 μm. Upon selectively resolving the sacrificial layer, the normal strain gradient in the titanium film caused an upward bending and rolling up of the complete layer system into a tubular geometry with a radial magnetic easy axis. Suitable microtubes were identified and characterized with scanning electron microscopy (SEM) and located in the MFM using external CCD cameras. The microtube discussed below is shown in fig. 2a. We use a NanoScan hr-MFM device supplemented by a Zurich Instruments HF2LI lock-in amplifier, and commercial cone-shaped Team Nanotec HR-MFM45 ML3 tips with a hard magnetic cobalt alloy coating and a nominal cantilever stiffness of 0.7 N/m. The resonance frequencies for fundamental and second mode flexural cantilever eigenoscillation were determined sweeping the excitation frequency and locating the resonance peaks in the amplitude spectrum. In order to reveal the position of the select microtube for subsequent magnetic imaging, large area overview maps of the fundamental mode frequency shift were performed. For this purpose a high DC bias voltage of 3 V was applied between tip and sample leading to a strong electrostatic field gradient, which dominates the frequency shift even for tip-sample distances $> 6\,\mu$m. A PLL-controlled AC

voltage with a frequency f_{AC} equal to half the second flexural eigenmode of the cantilever and a peak amplitude of $\hat{U}_{AC} = 1.0\,V$ was applied between tip and sample. We minimized electrostatic contrast in MFM images through compensating the contact potential between tip and sample surface via an additional DC tip-sample bias voltage. After aligning the scan area to cover the major part of the microtube surface, the center point of the MFM scan area is used to determine the contact potential difference by sweeping the DC bias at a fixed tip-sample distance of $(205 \pm 10)\,\mathrm{nm}$, see fig. 2b.

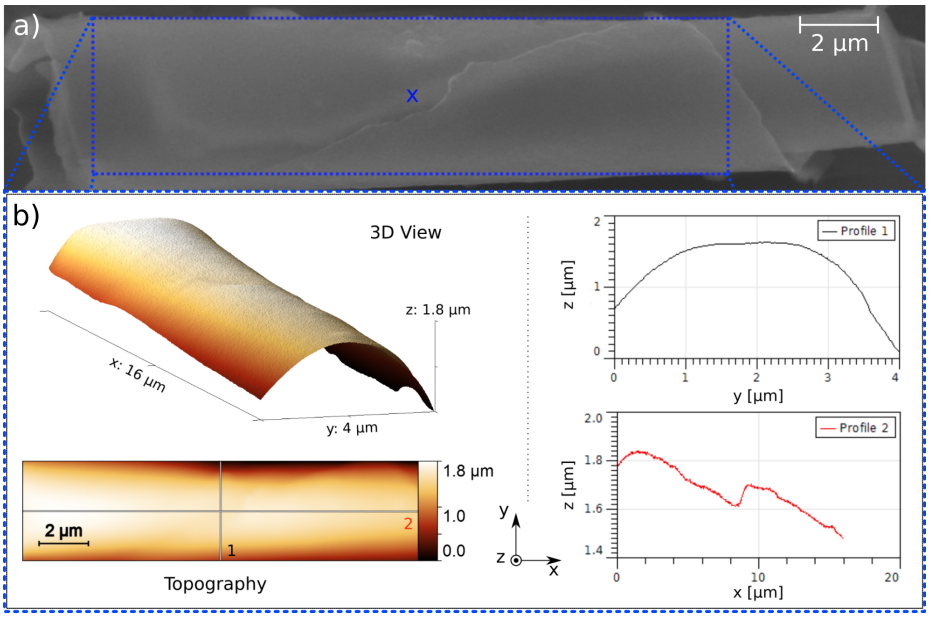

Figure 2: a) SEM image of a Co/Pd microtube with two windings: Blue drawn box with center point (x) shows the range of the MFM scan, representing an area of $16\,\mu\mathrm{m} \times 4\,\mu\mathrm{m}$. b) MFM topographic channel, recorded in zero-field from top left to bottom right at a tip-surface distance of $(205 \pm 10)\,\mathrm{nm}$, with the latter measured above the center point. In this experiment, $A_2 = 0.22\,\mathrm{nm}$, if $\hat{U}_{AC}$=1.0 V is applied between MFM tip and sample. Shown are 3D and top view topographic images with two line profiles across the tube circumference (profile 1) and along the tube axis (profile 2). Profile 2: A step in the tube topography is visible which originates from the edge of the outer winding that is wrapped around the inner winding with a spacing of approximately 100 nm.

Prior to MFM measurements, the microtube was saturated in an external magnetic field perpendicular to the image plane at -430 $\frac{\mathrm{mT}}{\mu_0}$. The field was provided by a calibrated perpendicular field device based on a cylinder-shaped NdFeB permanent magnet. For field dependent measurements, the field direction was rotated by 180° to enable fields with opposite polarity. In-field measurements were performed at incremental steps up to a final field of 400 $\frac{\mathrm{mT}}{\mu_0}$. The remanent state was recorded after reaching a maximum field of 430 $\frac{\mathrm{mT}}{\mu_0}$.

Fig. 3 shows a selection of several frequency shift maps that form the basis for a detailed evaluation of the local magnetization reversal process in the microtube. At 60 $\frac{\mathrm{mT}}{\mu_0}$, the first reversed domain emerges, whose magnetization is aligned along the applied field direction. As the magnetization of this domain and the tip magnetization are oriented almost parallel to each other, the detected attractive magnetostatic interaction between them leads to a negative frequency shift Δf_1 in the local MFM response. The location of the first reversed domain is characterized by two features: It

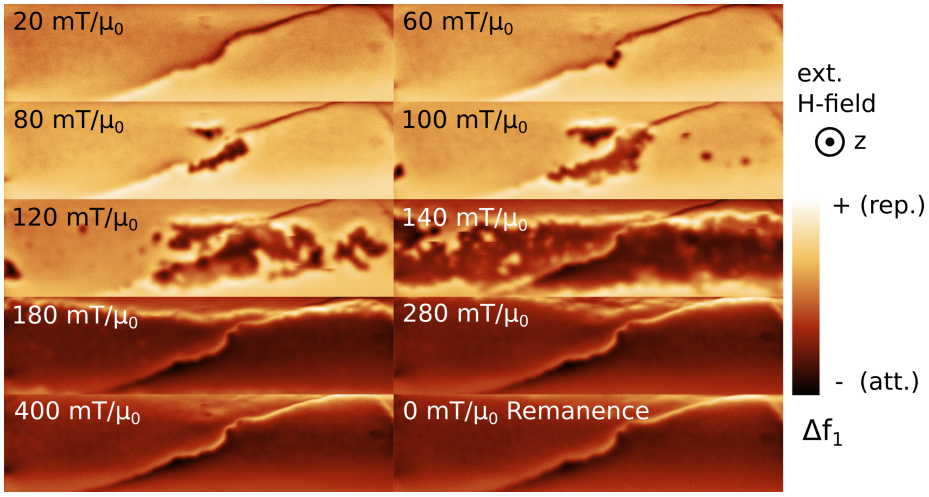

Figure 3: Fundamental mode frequency shift (Δf_1) maps showing the magnetostatic interaction (repulsive/attractive) between MFM tip and microtube surface for different values of the applied magnetic field. A tip-surface distance of (205 ± 10) nm and a constant amplitude $A_1 = 10$ nm were used. The direction of the applied field is perpendicular to the image plane and points toward the reader. The tip magnetization is, in first approximation, oriented in the direction of the applied field. Dark (bright) contrast corresponds to attractive (repulsive) interaction. The magnetostatic contrast near the overlapping edge is expected in case of stray-fields near edges of perpendicularly magnetized thin films.

appears at the edge of the outer winding and the local surface normal is nearly parallel to the external field. At larger perpendicular fields between 100 $\frac{\mathrm{mT}}{\mu_0}$ and 120 $\frac{\mathrm{mT}}{\mu_0}$, more domains form predominantly in regions with the surface normal parallel to the external field, while existent attractive domains expand primarily along the tube axis. At 280 $\frac{\mathrm{mT}}{\mu_0}$, the magnetization reversal is nearly complete, except for some regions at the upper edge of the scanning range, which represent locations with large angles between external field and surface normal. The MFM maps at 400 $\frac{\mathrm{mT}}{\mu_0}$ and at the subsequent remanent state, after increasing the field to a maximum value of 430 $\frac{\mathrm{mT}}{\mu_0}$, look similar despite different anticipated magnetization configurations. Here, we assume a locally homogenous radial magnetization in the investigated microtube area at remanence, and a tilt of the magnetization toward the external magnetic field at 400 $\frac{\mathrm{mT}}{\mu_0}$.

The experimental results obtained from the rolled-up films were further compared with their planar counterparts to identify effects induced by rolling, e.g. 3D shape. For convenience, the planar film reversal was studied by polar magneto-optical Kerr effect (MOKE) microscopy [40] with normal magnetic field up to 1 $\frac{\mathrm{T}}{\mu_0}$ generated by a solenoid.

3 Statistical evaluation of magnetization status

For further quantitative analysis, the magnetization reversal process is statistically evaluated as a function of the surface orientation with respect to the external magnetic field. The procedure is first demonstrated on the example of the demagnetized state, set after decreasing an AC magnetic field applied perpendicularly to the sample substrate (fig. 4a).

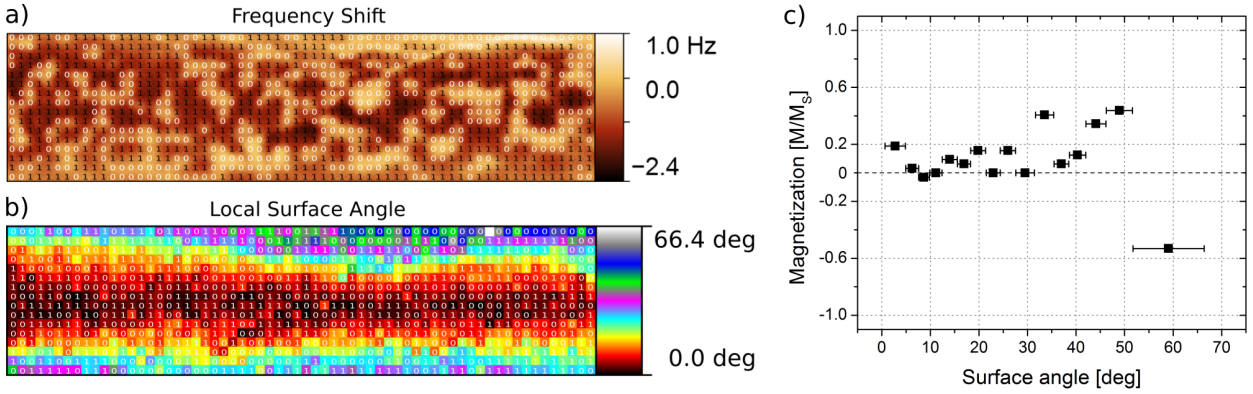

Figure 4: a) MFM frequency shift of the demagnetized state and b) surface angle map of the same microtube region as shown in figures 2 and 3. The numbers "0" and "1" shown in a) and b) refer to predominantly repulsive and attractive magnetostatic interactions, respectively. c) Angle-dependent normalized net magnetization: Every single data point corresponds to one specific angle interval, each containing 64 cells. The bars indicate the boundaries of the angle intervals. The net magnetization scatters around zero for most data points, i.e. $N_a \approx N_r$. For large angles above 46°, the net magnetization fluctuates heavily around zero.

Taking advantage of the perpendicular magnetic anisotropy of the magnetic film, the MFM frequency shift map (fig. 4a) can be translated to a radial magnetization configuration with bright and dark regions pointing inward and outward, respectively. To facilitate the evaluation of the local magnetization state, a matrix consisting of 64 x 16 cells was created using the original 1024 x 256 px data and placed on top of the MFM map. The switching status of each cell was determined with an ad-hoc ansatz: Cells with dominating bright and dark contrast were manually assigned to the magnetization status "0" (repulsive) and "1" (attractive), referring to a magnetization pointing inward and outward, respectively. According to W.M. Li et al. [41] a statistic estimate of the normalized net magnetization M/M_S of the sample region covered by the matrix or by specific parts of the matrix can be calculated as:

$$\frac{M}{M_s} = \frac{N_a - N_r}{N_a + N_r} \,. \tag{3}$$

Here N_a and N_r are the number of cells with attractive and repulsive magnetostatic interaction, indicated by dark and bright contrast in the MFM frequency shift map, respectively. M_S denotes the saturation magnetization. Fig. 4b shows a local surface angle map for the same matrix. We declare the term "surface angle" as the angle between the microtube surface normal and the perpendicular z-coordinate. In this notation, the surface angle is equivalent to the former definition of ϕ since the external magnetic field points along the z-axis. Note that the value of each pixel of the 64 x 16 px map in fig. 4b was determined by means of a nearest neighbor approximation using the original 1024 x 256 px data of surface angles between the local microtube surface normal and the direction of the perpendicular magnetic field. Next we form groups of cells with each group associated with an interval of surface angles. The angle intervals are calculated in two different ways: i) constant number of cells, i.e. $N_a + N_r = 64$, and variable interval size; ii) constant interval size, i.e. 5 degrees, and variable number of cells. For each angle interval the net magnetization is evaluated according to eq. 3.

The first approach is used to analyze the demagnetized state shown in fig. 4, and for the field-dependent measurements discussed below. Calculating the mean value of the magnetization states of all 1024 surface cells (see fig. 4) yields a normalized net magnetization of $M/M_S = 0.094$ for the entire MFM scan area, corresponding to a nearly demagnetized microtube. At larger surface angles, however, this evaluation method considerably deviates from the anticipated demagnetized state (see fig. 4c). This discrepancy is due to methodological challenges of MFM with detecting magnetic stray fields from domains at large surface angles and will be discussed later.

The same evaluation method based on surface angle intervals with a constant number of 64 cells is employed to analyze the magnetization reversal process beginning with the saturated remanent state of the microtube (MFM maps in fig. 3). Fig. 5a shows the angular dependence of the normalized net magnetization for various external fields. The second evaluation method is employed to determine the switching fields for one specific fixed angle interval size, and to estimate the field dependence of the normalized net magnetization (fig. 5b).

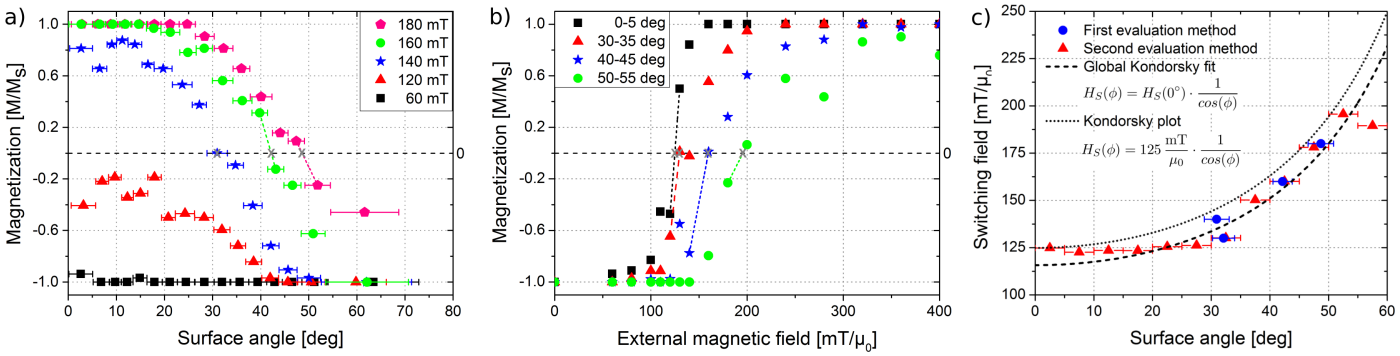

Figure 5: a) Normalized net magnetization according to eq. 3, for variable size of angle intervals and fixed number of cells. It is based on the evaluation of the magnetic stray field maps shown in fig. 3 and their respective surface angle maps. b) Field-dependent normalized net magnetization according to eq. 3, for constant size of angle intervals and variable number of cells. c) Angular dependence of the local switching field for the first (●) and second (▲) evaluation method. The data is fitted using the global Kondorsky-type $1/\cos(\phi)$ function and a modified version based on an experimentally determined $H_S(0°) = 125\ \frac{\mathrm{mT}}{\mu_0}$.

Note the synonymous use of "magnetic switching field" and "magnetic coercivity" at the local scale in the investigated perpendicularly magnetized films. The approximated states with zero net magnetization are retrieved by linear interpolation (figs. 5a,b). Hence, in the second evaluation method the field resolution is not limited to the predefined magnetic field steps. The occurrence of additional data points (▲) in the surface angle range $0° - 30°$ (fig. 5c) makes the second method more suited to determine the switching field at small surface angles, paying tribute to the shallow slope of the Kondorsky function at small angles.

The following paragraph is dedicated to challenges of MFM with detecting magnetic stray fields from domains at large surface angles. Considering the extreme case of $\phi = 90°$, a horizontally aligned cantilever oscillating in the z-direction translates to an in-plane oscillation with respect to the surface plane. In this case, the measured z-derivative of the magnetostatic force corresponds to a local in-plane MFM measurement similar to MFM in pendulum geometry [42, 43]. Hence, magnetic domains

separated by domain walls parallel to the tip oscillation do not contribute to an MFM signal due to absent z-derivatives of the stray field components along this direction (fig. 6a). Although the internal structure of domain walls, i.e. domain wall type, dictates the longitudinal component of the local magnetization, the latter does not directly translate to a longitudinal stray field component. Namely, Bloch walls observed in symmetric Co/Pd multilayers [12] generate a longitudinal magnetization [9], parallel to the z-direction discussed here; Néel walls cause a perpendicular component at the expense of a longitudinal one [9]. Either wall has a normal (radial) stray field component but lacks a longitudinal contribution for absent Bloch lines. In contrast, domain walls perpendicular to the tip oscillation (fig. 6b) generate stray field z-components with corresponding z-derivatives and emergent MFM contrast. To minimize these systematic uncertainties at large ϕ, we limited the analysis of the MFM data to surface angles $\phi < 60°$.

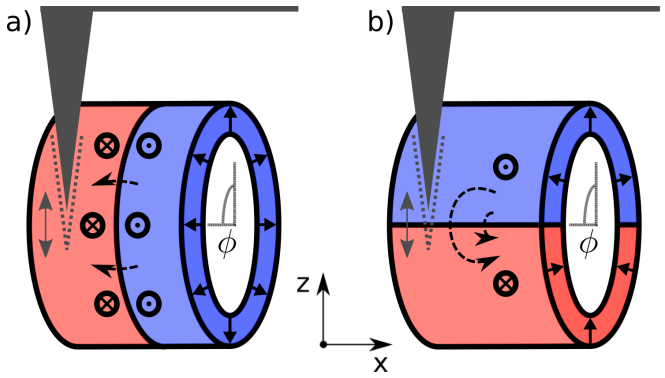

Figure 6: Sketch of the extreme case where the MFM tip oscillates parallel to the local microtube surface ($\phi = 90°$) with two different simplified magnetic domain configurations. a) For domain walls parallel to the tip oscillation direction, no MFM signal is expected due to vanishing magnetostatic force z-component. b) Domain walls perpendicular to the tip oscillation cause a detectable MFM signal.

4 Results and Discussion

Possible modifications to static properties of rolled-up magnetic nanomembranes with respect to their initial planar configuration include strain relaxation (reduced magnetostrictive anisotropy), curvature effects (chirality selection), topology-induced domain patterning, and radial/vertical repetition (increased saturation magnetization). Neither of those cases is valid in our study. Firstly, the titanium film is heavily strained and relaxes upon rolling without noticeable effect on the magnetic properties of the Co/Pd multilayer stack. Secondly, curvature effects, such as magnetochirality and vector spin exchange, require substantially smaller radii, i.e. 50 nm, to compete with the governing scalar Heisenberg exchange interaction. This leaves the two scenarios of topology-induced domain patterning and modification to remanent state, switching field, and saturation magnetization. In a previous work, we reported that both cases surface in tightly wound tubular nanomembranes [12]. Our analysis shows that such a modification indeed requires tightly wound layers, otherwise leading to microtubes with properties very similar to their planar counterparts.

A fully saturated remanent state after exposing to a normal magnetic field of 430 $\frac{\mathrm{mT}}{\mu_0}$ suggests a reduced magnetostatic coupling between adjacent windings due to loosely wound nanomembrane.

In fact, a comparison of the magnetization reversal process, including the normal switching field $H_S(0°)$, between the present microtube and a planar Co/Pd multilayer film with very same initial properties reveals a value of 125 $\frac{\mathrm{mT}}{\mu_0}$ for the angle range of 0 - 5° and $H_S(0°) = (127 \pm 4)\,\frac{\mathrm{mT}}{\mu_0}$, respectively. Measurements on a second microtube with comparable geometry yield $H_S(0°) = 129\,\frac{\mathrm{mT}}{\mu_0}$. The imperfect rolling up is evident in the SEM micrograph as well as in the topography scan revealing a profile with a 100 nm high step (fig. 2) corresponding to the spacing between adjacent Co/Pd multilayer films. Fitting the Kondorsky relation to the experimental data to describe their angular dependence yields a slightly lower switching field of $H_S(0°) = (116 \pm 2)\,\frac{\mathrm{mT}}{\mu_0}$ (fig. 5c). For comparison, an additional Kondorsky plot with $H_S(0°)$ fixed to the experimentally determined value of 125 $\frac{\mathrm{mT}}{\mu_0}$ is displayed. It is obvious that the unmodified Kondorsky function with one more variable fits fairly well to experimental data. The validation to treat this angular dependence with the unmodified Kondorsky function is given by a substantially smaller switching field $H_S(0°)$ compared to the anisotropy field $H_a = 2K_u/M_S$ generated by the perpendicular magnetic anisotropy K_u in the ferromagnetic material [44]. Taking into account typical material parameters for the measured Co/Pd thin film, i.e. $K_u = 200\,\mathrm{kJ/m^3}$ and $M_S = 500\,\mathrm{kA/m}$ [45], we obtain $H_a = 800\,\frac{\mathrm{mT}}{\mu_0}$, which is more than six times larger than $H_S(0°) = 125\,\frac{\mathrm{mT}}{\mu_0}$. For similar $H_S(0°)$ and H_a, the angular dependence of the switching field deviates from the simple $1/\cos(\phi)$ relation and requires modification to the Kondorsky function [28, 44]. Switching fields larger than the anisotropy field transform the Kondorsky-type character into a Stoner-Wohlfarth-like behavior (fig. 1). This implies in particular that the minimal switching field $H_{S,\mathrm{min}}$ is not located at 0°. For instance, H_S is minimal at 45° if $H_S(0°)$ equals H_a [44]. In the present case (fig 5c), the minimal switching field is $H_{S,\mathrm{min}} = H_S(7.5°) = 123\,\frac{\mathrm{mT}}{\mu_0}$. Both location and reduction with respect to $H_S(0°)$ are confirmed in a second microtube ($H_{S,\mathrm{min}} = H_S(7.5°) = 127\,\frac{\mathrm{mT}}{\mu_0}$). Together with an apparent delayed onset of the Kondorsky relation, this finding indicates a minor yet noticeable Stoner-Wohlfarth-like contribution. The governing mechanism of a pinning site dominated magnetization reversal is reflected in fig. 3, where the switching begins in the central region of the microtube and stops at large surface angles. In these border regions, the domain walls are pinned and do not move until a larger field is applied sufficient to push the domain wall further toward regions with even higher surface angles.

5 Summary and Outlook

We spatially resolved the magnetization reversal process in radially magnetized loosely wound tubular geometries facilitating multi-frequency magnetic force microscopy. On the microscale due to absent magnetostatic interwinding coupling, the rolled-up nanomembrane behaves like a planar film with perpendicular magnetic anisotropy, whose angular dependence of the switching field can be described by the Kondorsky model. This field dependence agrees well with previous works on tightly wound microtubes using magnetic x-ray tomography. The present work is a first demonstration of multi-frequency MFM as a versatile microscopy tool to investigate field-dependent magnetization processes at the nanoscale on curved surfaces with large slopes. The fundamental limitation of MFM contrast formation in case of large surface angles $\phi \approx 90°$ can be overcome utilizing advanced MFM probes and modes of operation that offer multi-directional tip oscillations. Based on its performance and potential, we envision that multi-frequency MFM will emerge as a cost-efficient table-top tool with essential contributions to 3D nanomagnetism, complementing high-resolution Lorentz microscopy,

vector field electron tomography, and magnetic x-ray microscopy and tomography requiring large-scale user facilities.

6 Acknowledgements

We would like to acknowledge Stefan Pofahl and Ivan Soldatov for providing Kerr measurements and to Gesine Kreutzer for assistance with the SEM. We also want to thank Paolo Navaretti from Zurich Instruments for giving technical support concerning the lock-in device.

This project has been supported by the DFG (Grant No. MU 1794/3-2 and SFB 1143/C05).

R. S. acknowledges support from the U.S. Department of Energy, Office of Science, Basic Energy Sciences, Materials Sciences and Engineering Division under Contract No. DE-AC02-05-CH11231 within the NEMM program (MSMAG).

7 References

[1] A. Fernández-Pacheco, R. Streubel, O. Fruchart, R. Hertel, P. Fischer, and R. P. Cowburn. Three-dimensional nanomagnetism. *Nat. Commun.*, 8(15756), 2017.

[2] R. Streubel, P. Fischer, F. Kronast, V. P. Kravchuk, D. D. Sheka, Y. Gaididei, O. G. Schmidt, and D. Makarov. Magnetism in curved geometries. *J. Phys. D: Appl. Phys.*, 49(363001):45pp, 2016.

[3] Y. Gaididei, V. P. Kravchuk, and D. D. Sheka. Curvature effects in thin magnetic shells. *Phys. Rev. Lett.*, 112(257203), 2014.

[4] R. Hertel. Curvature-induced magnetochirality. *SPIN*, 03(1340009), 2013.

[5] M. Yan, S. Gliga A. Ka'kay, and R. Hertel. Beating the walker limit with massless domain walls in cylindrical nanowires. *Phys. Rev. Lett.*, 104(057201), 2010.

[6] D. Karnaushenko, D. D. Karnaushenko, D. Makarov, S. Baunack, R. Schäfer, and O. G. Schmidt. Self-assembled on-chip-integrated giant magneto-impedance sensorics. *Adv. Mater*, 27(6582-6589), 2015.

[7] T. Ueltzhöffer, R. Streubel, I. Koch, D. Holzinger, D. Makarov, O. G. Schmidt, and A. Ehresmann. Magnetically patterned rolled-up exchange bias tubes: A paternoster for superparamagnetic beads. *ACS Nano*, 10(9):8491–8498, 2016.

[8] S. S. P. Parkin, M. Hayashia, and L. Thomas. Magnetic domain-wall racetrack memory. *Science*, 320, 2008.

[9] R. Streubel, C.-H. Lambert, N. Kent, P. Ercius, A. T. N'Diaye, C. Ophus, S. Salahuddin, and P. Fischer. Experimental evidence of chiral ferrimagnetism in amorphous GdCo films. *Adv. Mater.*, 30(1800199), 2018.

[10] C. Phatak and A. K. Petford-Long. Three-dimensional study of the vector potential of magnetic structures. *Phys. Rev. Lett.*, 104(253901), 2010.

[11] T. Tanigaki, Y. Takahashi, T. Shimakura, T. Akashi, R. Tsuneta, A. Sugawara, and D. Shindo. Three-dimensional observation of magnetic vortex cores in stacked ferromagnetic discs. *Nano Lett.*, 15:1309–1314, 2015.

[12] R. Streubel, F. Kronast, P. Fischer, D. Parkinson, O. G. Schmidt, and D. Makarov. Retrieving spin textures on curved magnetic thin films with full-field soft X-ray microscopies. *Nat. Commun.*, 6(7612), 2015.

[13] C. Donnelly, M. Guizar-Sicairos, Valerio Scagnoli, S. Gliga, M. Holler, J. Raabe, and L. J. Heyderman. Three-dimensional magnetization structures revealed with x-ray vector nanotomography. *Nature*, 547(328), 2017.

[14] D. Sanz-Hernández, R. F. Hamans, J.-W. Liao, A. Welbourne, R. Lavrijsen, and A. Fernández-Pacheco. Fabrication, detection, and operation of a three-dimensional nanomagnetic conduit. *ACS Nano*, 11:11066–11073, 2017.

[15] H. A. M. de Gronckel, C. H. W. Swüste, K. Kopinga, and W. J. M. de Jonge. Microscopic properties of Co/Pd multilayers studied by ferromagnetic and nuclear magnetic resonance. *Appl. Phys. A*, 49:467–472, 1989.

[16] T. Yang, F. Pan, and B. X. Liu. Microstructure and magnetic properties of Co/Pd multilayer films. *phys. stat. sol. (a)*, 142(443), 1994.

[17] H. J. G. Draaisma, F. J. A. den Broeder, and W. J. M. de Jonge. Perpendicular anisotropy in Pd/Co multilayers. *J. Appl. Phys.*, 63(3479), 1988.

[18] C. F. Reiche, S. Vock, V. Neu, L. Schultz, B. Büchner, and T. Mühl. Bidirectional quantitative force gradient microscopy. *New J. Phys.*, 17(013014), 2015.

[19] T. Mühl, J. Körner, S. Philippi, C. F. Reiche, A. Leonhardt, and B. Büchner. Magnetic force microscopy sensors providing in-plane and perpendicular sensitivity. *Appl. Phys. Lett.*, 101(112401), 2012.

[20] E. C. Stoner, F. R. S., and E. P. Wohlfarth. A mechanism of magnetic hysteresis in heterogeneous alloys. *Philos. Trans. R. Soc. Lond. A*, 240(826):599–642, 1948.

[21] C. Tannous and J. Gieraltowski. The Stoner-Wohlfarth model of ferromagnetism. *Eur. J. Phys.*, 29:475–487, 2008.

[22] A. Aharoni and S. Shtrikman. Magnetization curve of the infinite cylinder. *Phys. Rev.*, 109(5):1522–1528, 1958.

[23] W. F. Brown. Micromagnetics, domains, and resonance. *J. Appl. Phys.*, 30(S62), 1959.

[24] R. Ferré, K. Ounadjela, J. M. George, L. Piraux, and S. Dubois. Magnetization processes in nickel and cobalt electrodeposited nanowires. *Phys. Rev. B*, 56(21), 1997.

[25] N. A. Usov, A. P. Chen, A. Zhukov, and J. González. Nucleation field of a soft magnetic nanotube with uniaxial anisotropy. *J. Appl. Phys.*, 104(083902), 2008.

[26] E. Kondorski. On the nature of coercive force and irreversible changes in magnetisation. *Phys. Z. Sowjet.*, 11:597, 1937.

[27] E. Kondorski. On hysteresis in ferromagnets. *J. Phys. (Moscow)*, II(2):161–181, 1940.

[28] C. H. Y. Deng and H. L. Huang. Domain wall structure and the modified Kondorsky function. *Chinese J. Phys.*, 39(5), 2001.

[29] W. Wernsdorfer, C. Thirion, N. Demoncy, H. Pascard, and D. Mailly. Magnetization reversal by uniform rotation (Stoner-Wohlfarth model) in f.c.c. cobalt nanoparticles. *J. Magn. Magn. Mater.*, 242-245 Part 1:132–138, 2002.

[30] M. Delalande, J. de Vries, L. Abelmann, and J. C. Lodder. Measurement of the nucleation and domain depinning field in a single Co/Pt multilayer dot by anomalous Hall effect. *J. Magn. Magn. Mater.*, 324:1277–1280, 2012.

[31] J. M. D. Coey. *Magnetism and Magnetic Materials.* Cambridge University Press, 2010.

[32] D. Roy and P. S. A. Kumar. Control of magnetization reversal in oriented strontium ferrite thin films. *J. Appl. Phys.*, 115(073906), 2014.

[33] J. Schwenk, X. Zhao, M. Bacani, M. Marioni, S. Romer, and H. J. Hug. Bimodal magnetic force microscopy with capacitive tip-sample distance control. *Appl. Phys. Lett.*, 107(132407), 2015.

[34] T. R. Albrecht, P. Grütter, D. Horne, and D. Rugar. Frequency modulation detection using high-Q cantilevers for enhanced force microscope sensitivity. *J. Appl. Phys.*, 69(2), 1991.

[35] J. Lohau, S. Kirsch, A. Carl, G. Dumpich, and E. F. Wassermann. Quantitative determination of effective dipole and monopole moments of magnetic force microscopy tips. *J. Appl. Phys.*, 86(3410), 1999.

[36] D. Ziegler and A. Stemmer. Force gradient sensitive detection in lift-mode Kelvin probe force microscopy. *Nanotechnology*, 22, 2011.

[37] B. I. Kim. Separation of topographic features from magnetic force images using capacitive coupling effect. *Rev. Sci. Instrum.*, 80(023702), 2009.

[38] J. Zarpellon, H. F. Jurca, J. Varalda, C. Deranlot, J. M. George, M. D. Martins, S. O. Parreiras, C. Müller, and D. H. Mosca. Magnetic domains in rolled-up nanomembranes of Co/Pt multilayers with perpendicular magnetic anisotropy. *RSC Adv.*, 4(8410), 2014.

[39] R. Streubel, J. Lee, D. Makarov, M.-Y. Im, D. Karnaushenko, L. Han, R. Schäfer, P. Fischer, S.-K. S.-K. Kim, and O. G. Schmidt. Magnetic microstructure of rolled-up single-layer ferromagnetic nanomembranes. *Adv. Mater.*, 26:316–323, 2014.

[40] J. Kerr. On rotation of the plane of polarization by reflection from the pole of a magnet. *Philos. Mag.*, 3(19):321–343, 1877.

[41] W. M. Li, Y. Yang, Y. J. Chen, T. L. Huang, J. Z. Shi, and J. Ding. Study of magnetization reversal of Co/Pd bit patterned media by micro-magnetic simulation. *J. Magn. Magn. Mater.*, 324:1575–1580, 2012.

[42] A. DiCarlo, M. R. Scheinfein, and R. V. Chamberlin. Magnetic force microscopy utilizing an ultrasensitive vertical cantilever geometry. *Appl. Phys. Lett.*, 61(2108), 1992.

[43] K. Kim, Y. Seo, H. Jang, S. Chang, M. Hong, and W. Jhe. Shear-mode magnetic force microscopy with a quartz tuning fork in ambient conditions. *Nanotechnology*, 17(201), 2006.

[44] F. Schumacher. On the modification of the Kondorsky function. *J. Appl. Phys.*, 70(3184), 1991.

[45] R. Streubel, P. Fischer, M. Kopte, Oliver G. Schmidt, and Denys Makarov. Magnetization dynamics of imprinted non-collinear spin textures. *Appl. Phys. Lett.*, 107(112406), 2015.